Soft Matter

REVIEW

View Article Online
View Journal | View Issue

Cite this: *Soft Matter*, 2017, **13**, 37

Clogging of microfluidic systems

Emilie Dressaire*[a] and Alban Sauret[ab]

Received 14th August 2016,
Accepted 18th October 2016

DOI: 10.1039/c6sm01879c

www.rsc.org/softmatter

The transport of suspensions of microparticles in confined environments is associated with complex phenomena at the interface of fluid mechanics and soft matter. Indeed, the deposition and assembly of particles under flow involve hydrodynamic, steric and colloidal forces, and can lead to the clogging of microchannels. The formation of clogs dramatically alters the performance of both natural and engineered systems, effectively limiting the use of microfluidic technology. While the fouling of porous filters has been studied at the macroscopic level, it is only recently that the formation of clogs has been considered at the pore-scale, using microfluidic devices. In this review, we present the clogging mechanisms recently reported for suspension flows of colloidal particles and for biofluids in microfluidic channels, including sieving, bridging and aggregation of particles. We discuss the technological implications of the clogging of microchannels and the schemes that leverage the formation of clogs. We finally consider some of the outstanding challenges involving clogging in human health, which could be tackled with microfluidic methods.

1 Introduction

Suspensions of microparticles occupy an important place in industrial and biological systems as the liquid phase allows the transport of the solid matter.[1–6] Despite the wide use of suspensions of rigid or deformable particles, the understanding of the processes governing their flow in confined environments remains limited due to the complexity of the particle motions and interactions. In this review, we are interested in the clogging transition, *i.e.*, the mechanisms that interrupt the transport of particles in confined geometries. In some situations, the formation of clogs can be desirable, for instance to reinforce porous and fractured substrates such as concrete and rocks[7,8] or for the detection of biological cells.[9] However, in many applications clogs decrease the lifetime and efficiency of micro-engineered systems that are used for the fabrication, transport and analysis of fluid samples. For example, some microfluidic processes rely on microparticles to selectively bind to target molecules or cells,[10]

[a] *Department of Mechanical and Aerospace Engineering, New York University Tandon School of Engineering, Brooklyn, NY 11201, USA. E-mail: dressaire@nyu.edu*
[b] *Surface du Verre et Interfaces, UMR 125 CNRS/Saint-Gobain, 93303 Aubervilliers, France*

Emilie Dressaire

Emilie Dressaire graduated from ESPCI in Paris, in 2005. She obtained her PhD in mechanical engineering from Harvard University in 2009. Before joining New York University, she served on the faculty at Trinity College and as a postdoctoral fellow at McGill University. She is now an Assistant Professor of Mechanical Engineering at the NYU Tandon School of Engineering. Her research interests involve fluid dynamics and soft matter science.

Alban Sauret

Alban Sauret is a Research Scientist at CNRS in France, where he worked at SVI, a joint laboratory between CNRS and Saint-Gobain. He is also a visiting Researcher at NYU Tandon School of Engineering. Previously, he studied at ENS Lyon, then Aix-Marseille University in France, before doing a postdoc at Princeton University. His research aims at understanding the couplings between the fluid dynamics, interfacial effects and particle transport mechanisms involved in environmental, industrial and geophysical processes.

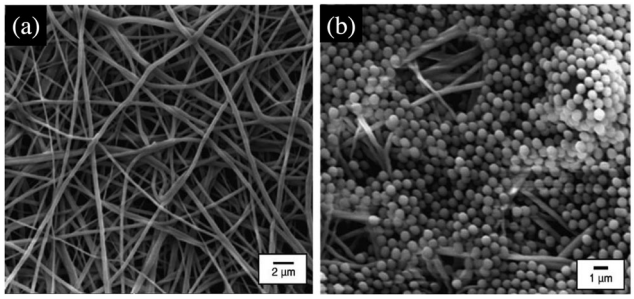

Fig. 1 Images of electrospun nanofibrous membranes obtained with a field-emission scanning electron microscope.[21] (a) Before filtration and (b) after filtration of a suspension of 1 μm polystyrene particles. Reprinted with permission from *J. Membr. Sci.*[21] Copyright 2006 Elsevier.

to carry chemicals[11] or to stabilize emulsions.[12] Other microfluidic devices are engineered for pure fluid samples that accidentally get contaminated with impurities or suspended particles. Similarly, common macroscopic technological and biological processes involve the micro-flow of suspensions through complex networks of channels, including the filtration of water through porous membranes as illustrated in Fig. 1,[13–15] the flow of ink in printers[16,17] or the transport of blood cells within the microvascular system.[18–20]

The flow behavior of a suspension of hard spheres has been described at low solid volume fraction, below the jamming transition.[1,2,22–24] The rheology of a suspension is strongly dependent on the solid fraction. At low solid fraction, the suspension behaves like a Newtonian fluid whose effective viscosity $\mu_{\text{eff}}(\phi)$ increases with the solid volume fraction ϕ, and can be described through the relation

$$\mu_{\text{eff}}(\phi) \approx \mu_0 \frac{\exp(-2.34\phi)}{(1-\phi/\phi_{\text{m}})^3}, \quad (1)$$

where μ_0 is the viscosity of the liquid phase and $\phi_{\text{m}} = 0.62$.[25] However as the suspension becomes dense, the behavior becomes more complex and there is a solid fraction beyond which the flow is no longer possible.[26–28] This jamming transition leads to the clogging of the system.

For particle concentrations below the jamming solid fraction, the formation of a clog is associated with complex local processes that cannot be captured through continuum rheological modeling. The description of such clogging processes has recently been the focus of a body of microfluidic research based on suspensions of microparticles whose typical diameter ranges between a hundred nanometers and a few micro-meters. Flows at the micrometer-scale are characterized by low Reynolds numbers, $\text{Re} = \rho U\ell/\mu$, where ρ and μ are the density and dynamic viscosity of the fluid, respectively, ℓ the lengthscale (width or height) of the channel and U the fluid velocity. The flow dynamics in such systems can therefore generally be described through the Stokes approximation.[29] In addition, the effects of diffusive, advective and colloidal forces on the particles result in the rich behavior of the suspension and the formation of clogs. The relative magnitude of Brownian and hydrodynamic effects is captured by the Peclet number: $\text{Pe} = 6\pi\mu D^2 U/k_{\text{B}}T$, where D is the diameter of the particles, U and μ are the velocity and dynamic viscosity of the fluid, respectively, k_{B} is the Boltzmann constant and T the absolute temperature. For micrometer-scale particles at room temperature, the critical flow velocity below which the diffusion velocity becomes comparable to the advection is of the order of 0.1 micrometer per second, which in most systems is only the case near contact at the wall and can therefore be neglected. In confined geometries, the combination of long range, steric and hydrodynamic interactions can lead to the capture of the particles on the walls of the microchannels. Particle trapping in low Reynolds number flows is exploited in industrial and natural processes including in filtration to improve the retention of solid matter.[4] The deposition of particles and their subsequent assembly can eventually induce the formation of a clog, *i.e.*, a single or multi-particle structure that spans over the cross section of the channel. When such a blockage occurs, it prevents further passage of the particles that build up a porous aggregate and reduce dramatically the flow rate of the fluid.

The early work of Wyss *et al.* established that microfluidic is a good method to study confined particle-laden flows and clogging at the pore-scale.[30] Microfluidic devices are commonly designed using Computer Assisted Drawing (CAD) software and fabricated through soft lithography techniques using a clear elastomer, such as polydimethylsiloxane (PDMS).[31] The simple design of the flow geometry, the low cost of the devices, and the ability to track particles with optical microscopy allow the investigation of canonical configurations to identify the relevant physical parameters and collect statistically meaningful data. This review focuses on the mechanisms of clog formation in microfluidic systems, at the pore-scale. Indeed recent advances in the flow of suspensions in confined environments rely in large part on the ability to precisely control the flow at the micrometer-scale and monitor the clogging dynamics at the pore or microchannel level. In this review, we discuss the formation of clogs in microchannels through the sieving of large particles, rigid or soft (Section 2), the jamming at constrictions (Section 3) and the clogging by aggregation of particles (Section 4) in microchannels. We focus on describing the main features of the three mechanisms represented schematically in Fig. 2. The important technological

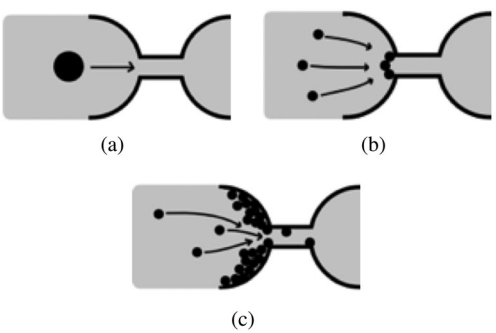

Fig. 2 Different mechanisms responsible for the clogging of microchannels at a constriction: (a) sieving, (b) bridging and (c) aggregation of particles. The mechanism(s) involved depend on the size of the particle compared to the constriction, the concentration of the suspension and the particle–wall and particle–particle interactions.

implications of clogging are discussed briefly in the relevant sections. While our review is focused on the microfluidic advances in the field of clog formation, the results presented should also provide interesting insights to the field of fouling science, which seeks to characterize the transport of particulate suspensions through complex porous structures. Finally, we summarize some of the recent work on bioclogging that constitutes a dynamic field of research both fundamental, to understand healthy and pathological clogging in biological systems and applied, to develop new diagnostic methods (Section 5).

2 Sieving: from rigid to deformable particles

Sieving refers to the blockage of particles based on size exclusion. The sieving of microparticles should however not be reduced to a simple geometrical problem, as the trapping of soft and anisotropic particles within a constriction is a complicated problem with challenging technological applications.

2.1 Sieving of rigid particles

The sieving of particles contributes to the separation of solid matter from the fluid phase in filtration processes.[34,35] The entrapment of micrometer-sized solid particles occurs when the width of the microchannel or the constriction, W, is equal or smaller than the particle diameter D, $W \leq D$. Several studies have demonstrated that particles get sieved out of suspension at the entrance of a microchannel or constriction through direct hydrodynamic transport[36,37] or after rolling on the solid surface.[38,39] This method is commonly used in microfluidic technology to filter contaminants or separate particles of different sizes.[40,41]

In practice, suspensions of particles are often polydisperse, either naturally[42] or as an artifact of common fabrication methods.[43,44] The size distribution is characterized by a mean diameter and a standard deviation. The sieving mechanism allows the selective trapping of the large particles, *i.e.*, those whose diameter D satisfies $D \geq W$. The clogging dynamic is thus controlled by the concentration of large particles and the flow rate in the channel.[32] The probability of clog formation is measured by the mean clogging time, which is the time interval between the onset of the flow and the clog formation. Experimental measurements of the clogging times as presented in Fig. 3(a) follow a Poisson distribution, which is indicative of a random process:

$$p(t_{\mathrm{clog}}) = \frac{1}{\langle t_{\mathrm{clog}} \rangle} \exp\left(-\frac{t_{\mathrm{clog}}}{\langle t_{\mathrm{clog}} \rangle}\right) \qquad (2)$$

where $\langle t_{\mathrm{clog}} \rangle = 1/(cQ)$ with c the concentration of large particles ($D \geq W$) and Q the flow rate in the microchannel. Measuring the distribution of clogging times in parallel microchannels is thus a simple and rapid method for characterizing the tail of the size distribution corresponding to large particle diameters, which is difficult to detect with standard dynamic light scattering techniques.[45]

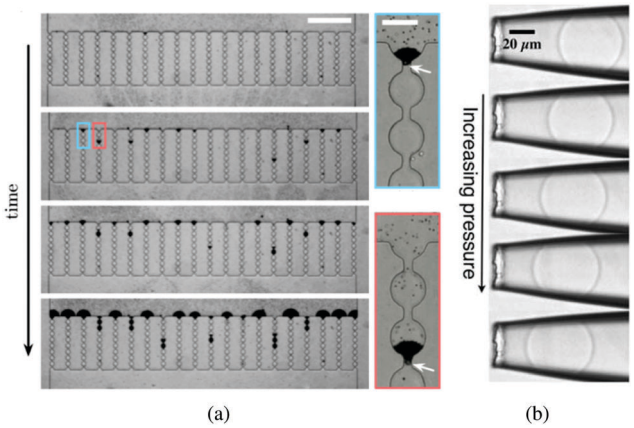

Fig. 3 (a) Time lapse of a typical sieving experiment in a device consisting of 20 parallel microchannels. Particles are black. After clogging, the particles accumulate and form a filter cake. The suspension flows from top to bottom (scale bar is 500 μm). The close-up views show the clog formed when a large contaminant blocks a microchannel at the entrance or further inside a microchannel. The white arrows indicate the position of the large contaminants (scale bar is 50 μm). Reprinted with permission from *Appl. Phys. Lett.*[32] Copyright 2014 AIP Publishing LLC. (b) Series of images of a microgel particle being deformed as the applied pressure increases; from top to bottom: p = 100, 150, 200, 250, 300 Pa. The fluid flow pushes the soft particle into the tapered capillary from right to left. Reprinted from *Soft Matter*.[33]

The trapping of anisotropic particles, such as fibers or ellipsoids, is possible if one of the particle dimensions exceeds the size of the channel. However, this geometrical criterion is not sufficient to determine whether a clog will form. The shape and initial orientation of the particle, the confinement and the geometry of the microchannel influence the probability and position of the clog.[46] In such systems, controlling the orientation of the particle as it approaches the constriction permits to determine the clogging probability. Once the interaction between the particle and the flow is well understood, it could be leveraged to open and close constrictions at will.

2.2 Sieving of a soft particle

The flow of soft deformable particles such as microspheres of elastomer, cells, and droplets is of great significance in the food and oil industries as well as in the biological and biomedical fields.[47–49] The mechanical behavior of suspensions of deformable particles leads to a wide range of flow properties. As opposed to solid particles, a soft particle can enter a microchannel whose size is smaller than the diameter of the particle at rest, $W < D$.[50–52]

When the flow across the channel is controlled by a pressure difference ΔP, both the volume and the shape of a deformable object change due to the local mechanical stresses. As ΔP increases, the particle dynamics can follow different scenarii: get trapped in the tapered or narrow entrance region of the microchannel [as shown in Fig. 3(b)], or flow through the channel when the pressure exceeds the translocation pressure noted ΔP_{max}.[53] The flow properties as well as the shape, the dimension and the mechanical features of the particle determine its behavior in

such a confined environment. For instance, healthy red blood cells, which are deformable, can flow through the microvascular system.[54,55] However, diseased blood cells, with reduced deformability can alter the blood flow and cause anemia and sepsis.[56,57] The change in mechanical behavior of the red blood cells is key to understand, diagnose and treat the associated diseases.

The flow and eventual trapping of a soft particle in a tapered capillary or axisymmetric microchannel with an opening angle α are commonly used to measure the mechanical properties of the particle [as illustrated in Fig. 3(b)].[33] Indeed the deformation of the particle is related to the elastic bulk (or compressive) and shear moduli of the material, noted K and G, respectively. Theoretically, the soft particle gets blocked when the pressure difference across the channel is lower than a threshold value. This latter can be estimated using a scaling approach to balance the deformation energy with the work of the pressure, assuming that the deformation of the particle is linearly elastic. The threshold value is thus defined as:

$$\Delta P_{\max} \propto E\left(\frac{D_0}{d_c}\right)^{14/3}, \tag{3}$$

where E and D_0 are the Young's modulus and the diameter of the particle at rest, respectively,[53] and the diameter of the microchannel is noted d_c. The coefficient of proportionality varies with the geometry of the inlet tapered region through its opening angle α.

For pressure values $\Delta P < \Delta P_{\max}$, the external mechanical stresses induced by the fluid balance the internal elastic stresses. The position of the stopped particle depends on the geometry of the tapered region and the particle, but also on the pressure drop imposed and the elasticity moduli (K, G).[33,58] Using a linear elastic description, and assuming that the opening angle α is smaller than about 15°, it is possible to describe the deformation of the particle at equilibrium using two parameters: the average radial strain, ε_r, and the average axial strain, ε_z, defined as

$$\varepsilon_r = -\frac{\Delta P}{G}\frac{6D_L{}^2 + \left(\frac{3K}{G} - 2\right)D_R{}^2}{18\frac{K}{G}(D_L{}^2 - D_R{}^2)}, \tag{4}$$

$$\varepsilon_z = 2\varepsilon_r\frac{3D_L{}^2 - \left(\frac{3K}{G} + 1\right)D_R{}^2}{6D_L{}^2 + \left(\frac{3K}{G} - 2\right)D_R{}^2}, \tag{5}$$

where D_L and D_R are the diameters of the particle on the left and right hand side of the contact zone with the microchannel wall.[52] To compute the position of the clog, one needs to know the geometry of the tapered region which prescribes the relation between the position of the particle and its geometry (ε_r, ε_z, D_L and D_R).

The formation of a clog by a soft particle in a tapered microchannel is a simple and accurate experimental method to measure the mechanical properties of individual micrometer-scale objects. This capillary micromechanics scheme has been applied to a variety of micrometer-scale objects, ranging from microgel[33] and core–shell particles[59] to cells.[60–64] We should emphasize that the modeling of the clogging of deformable particles in microchannels is particularly relevant to biological applications.

3 Bridging in microchannels

Clogging of a constriction can also occur when the diameter of the particles D is smaller than the size of the microchannel W. A first possible mechanism when $D < W$ is based on steric effects through the formation of an arch of particles across the width of the channel or constriction, which results in clogging. The combination of converging flow and high particle concentration generates bridge-like structures composed of a few particles, typically between 2 and 10, that span over the entire cross section of the channel.[65] Such blockages occur during the confined flow of hard spheres both in suspensions and in granular materials.[66–71] The latter situation has been studied in the silo geometry where dry grains are exiting a container through a small hole. Contrary to the clogging by sieving, the blockage by bridging is often intermittent as the arch can break under flow fluctuations.[72]

While bridges are often reported for local particle concentrations reaching the jamming value, studies have examined the creation of an arch upon the simultaneous arrival of particles at the channel opening for particle concentrations lower than the jamming value.[65,73] Beyond the fundamental implications of this work to describe the suspension rheology and jamming transition,[74–77] understanding and controlling the bridging occurrences can improve the processing of suspensions with a high solid fraction, encountered in industrial and technological systems. Intermittent bridging is particularly disruptive as it leads to local variations of the particle concentration.

3.1 Bridging of dense suspensions

The flow of dilute suspensions is well captured with a Newtonian description.[78,79] However, as the volume fraction of the particles increases, the rheology becomes more complex and the viscosity diverges near a critical or jamming volume fraction ϕ_m. For monodisperse hard spheres, the maximum packing fraction, $\phi \in [0.54,0.74]$, depends on the local arrangement. In addition, the flow of dense suspensions through confined environments can lead to local rearrangements of the particles and the formation of crystal structures.[80] In practice, the viscosity typically rises rapidly around $\phi = 0.5$ and diverges for $\phi_m = 0.585$ for hard spheres adopting a glass phase.[75,81] Jamming is therefore reported for dense suspensions, $\phi = 0.2$–0.6,[72,80,82,83] flowing through an increasingly confined environment in which the volume fraction locally reaches ϕ_m. For example, if $\phi < \phi_m$ in the microchannel, allowing for pressure driven flow, arches or force chains can form at a constriction when the combination of geometrical and hydrodynamic effects increases the volume fraction as illustrated in Fig. 4. This transition from continuous flow to arch formation occurs over a very small range of volume fractions, of the order of a few percents and results in a sharp decrease of the average

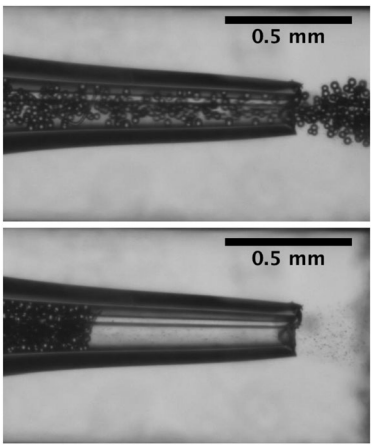

Fig. 4 Flow and clogging by bridging of a neutrally buoyant suspension of PMMA particles in an axisymmetric tapered glass capillary.

fluid velocity noted $\langle U \rangle$[72] and a decrease in particle concentration downstream due to the intermittent jamming.[83] This type of clogging occurs in a variety of systems in which a large number of particles, grains, pedestrians pass through a bottleneck.[70] Interestingly the analogy between those systems extends to their dynamics, as demonstrated by numerical simulations of colloidal suspensions using Lattice Boltzmann methods.[71] The simulations indicate that the time lapse between two consecutive bridging events follows a distribution with a power law tail, which is analogous to the flow of grains out of a hopper. Similarly, the number of particles released during the unjammed phase is well described by an exponential distribution.

Consistently, experimental work shows that the pressure driven flow of dense suspensions of hard particles leads to clogging if (1) a small number of particles can form a bridge across the width of the channel and (2) the flow velocity is above a threshold value noted U_{th}. For example, the clogging time, *i.e.*, the time between two consecutive bridging events is measured experimentally, and well captured by a power law:[84]

$$t_{\mathrm{clog}} \propto (\langle U \rangle - U_{\mathrm{th}})^{-\beta} \qquad (6)$$

for a suspension of poly(methyl methacrylate), PMMA particles ($\phi = 0.63$) flowing in a narrow microfluidic channel ($W = 20D$). The exponent $\beta \approx 0.34$ is obtained by fitting the experimental data to a power-law distribution. As the channel width increases, the fluctuations or bridging events become less regular and eventually disappear. Recent probabilistic models have shed light on the mechanism of arch formation but cannot yet predict the dynamics of suspension flows through a constriction.[70]

The intermittent nature of these clogs is due to the fragility of the bridged state: the arch can withstand large forces in only one direction, perturbations of the flow or small forces exerted in other directions can easily unjam the system. For example, the presence of rotating vortices prevents long-lived arches.[72] Taking advantage of the fragility of these arches will allow the development of self lubricating flow geometries, which could prevent the formation of clogs by bridging. In summary, the clogging by bridging for dense suspensions of microparticles shares common features with the clogging in a silo for a dry granular material.[70,71] However, contrary to dry grains flowing under gravity, suspensions of micrometer-scale particles can be diluted to few percents in a flowing liquid.

3.2 Arch formation in diluted suspension

Although generally associated to dense suspensions, bridging can also occurs for diluted suspensions at a small constriction. Indeed, arch formation has also been evidenced at $\phi \leq \phi_{\mathrm{m}}/10$.[65] The bridging results from the simultaneous arrival of particles that plug a cross section of the channel, typically at the inlet or at a constriction as shown by the example in Fig. 5. The probability of arch formation increases with the particle concentration, with the flow rate and with the ratio of the particle to the channel size D/W.[73,85] The complex bridging mechanism for diluted suspensions of microparticles is yet to be fully characterized. Several types of particle assemblies can constitute a stable arch, capable of interrupting the transport of particles (Fig. 5). Each of these assemblies is composed of a given number of particles arranged through the cross section. To determine the probability of formation of each assembly, it is necessary to account for both the initial position of the particles and the hydrodynamic forces as they determine the particle trajectories toward the constriction. If the particles approach the channel simultaneously, near contact, interactions involving the lubrication flow and interparticle forces determine whether an arch forms.[73,86] In first approximation, it is convenient to consider an axisymmetric channel. The monodisperse suspension of particles of diameter D has a solid volume fraction ϕ. The suspension enters a constriction through a circular opening of area A, smaller than the cross section of the channel. Assuming that the particles are advected at the speed of the fluid, a clog forms when the number of particles arriving simultaneously at the opening is larger that a critical number, noted n_{max}, defined empirically as:[87]

$$n_{\mathrm{max}} \propto \frac{AD}{2V_{\mathrm{p}}} \qquad (7)$$

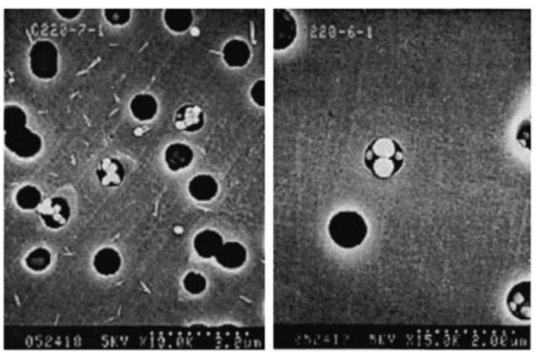

Fig. 5 Particle arches formed at high flow velocity. Negatively charged 0.249 μm diameter polystyrene sulfate particles flow through 1 μm pores. Reprinted with permission from *J. Fluid Mech.*[73] Copyright 2000 Cambridge University Press.

where $V_p = \pi D^3/6$ is the volume of a particle. The clogging time, which is the time interval between two arches form is predicted to be between a lower and an upper boundary:

$$\frac{(n_{max}/2+1)!}{(n_{max}\phi)^{n_{max}/2+1}}\frac{AD}{2Q} \leq t_{clog} \leq \frac{(n_{max}+1)!}{(n_{max}\phi)^{n_{max}+1}}\frac{AD}{2Q}, \quad (8)$$

where Q is the flow rate through the unobstructed constriction. This model is based on the assumption that the particles are initially uniformly distributed in the suspension and that clogging occurs when the number of particles arriving almost simultaneously at the opening, exceeds the critical value n_{max}. The particle trajectories can be defined more precisely by including the effects of buoyancy and inertia.[88] Although the approach is simplified, experimental results are in good agreement with the model.[87]

Recent work has shown that particle surface properties, and therefore particle–particle and particle–wall interactions modify the clogging dynamics. Experimentally, the ionic strength of the solution allows tuning the surface interactions.[89] For example, the presence of attractive interactions between particles facilitates the formation of the bridge but can also lead to the formation of aggregates. The growth of clusters of particles and the resulting blockage of the microchannel are discussed in the following section.

4 Clogging by aggregation

Whereas the two clogging mechanisms described previously, sieving and bridging, involve steric effects only, we now consider the clogging of a microchannel by successive deposition of colloidal particles. The self assembly of colloidal particles into clusters can occur in the bulk of a suspension or on a fluid interfaces.[90] Driven by short-range attractive van der Waals forces, this aggregation is only possible if the particles are at close enough distance to one another. In flowing suspensions, a particle can reach the vicinity of another particle or of the surface of the channel through advection or diffusion, depending on the Peclet number. The dynamics of the clogging process by aggregation of particles thus result from the combination of hydrodynamic and surface forces, as first reported in porous media.[13,15,91] Recent work on particle deposition and aggregation employs microfluidic to control the suspension flow and characterize the time evolution of the particle build-up.[30,37,92–95] Several studies have focused on the characteristic timescale of the blockage of the pore.[30,96,97] At low Reynolds number, as typically encountered in microfluidic channels, experiments indicate that a critical number of particles flow through the microchannel before the aggregate invades the cross section, thus preventing further passage of particles. Recent experimental work aims at describing the individual steps of the clogging process. Indeed the capture of the first particle and the growth of the aggregate determine the clogging dynamics, as the probability of deposition of individual particles varies over the different stages of the process.[14,38,92,97,98] Building on those observations, quantitative models now capture some features of the clogging process but various questions remain, including on the formation of a aggregate in three dimensions around the first layer of deposited particles.

4.1 Deposition of a single particle

The deposition of a single particle on the wall of a microchannel is the first step toward aggregation and clogging (see Fig. 6(a) and (f)). Numerical and experimental studies indicate that individual particles are preferentially captured at the entrance of the channel.[37,38,85,96,99] In microfluidic devices, the particle deposition process can be quantified through the surface coverage of the wall, which is defined as the surface area covered by particles divided by the total surface area. When the coverage is low, the deposition events can be treated as independent. The flux of particle deposition at the wall decreases with the distance from the entrance of the channel, with the Reynolds number of the flow and with the particle size.[100] The nature and intensity of the particle–wall interactions influence the rate of deposition in a complex way. Indeed, the surface forces between a particle and a wall are a combination of attractive van der Waals and repulsive electrostatic double layer interactions.[101] The relative magnitude of these two forces and the resulting energy profile depend on the physico-chemical properties of the particle and the wall, and the nature of flowing phase through its composition, pH and electrolyte concentration.[101] Experiments in microfluidic devices show that varying the concentration of the electrolyte typically sodium chloride, NaCl, can modify the deposition flux of particles at the wall by a factor 2.[100,102]

Two types of deposition behavior are reported. When the interactions between the particles and the wall are attractive for all separation distances, the deposition is favorable and the deposition flux, j_{dep} is large, typically with a wall coverage of the order of 10% after 30 minutes of flow for a suspension of 0.25 μm-latex particles at Re = 30 and $\phi = 1.31 \times 10^{-5}$ in a solution of NaCl (C = 0.01 M).[100,103] When the energy profile presents a repulsive region, the deposition is unfavorable, and the flux is lower.[100,104] In the latter case, the particle capture is

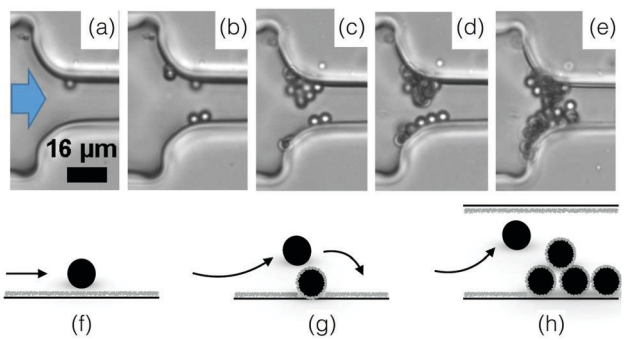

Fig. 6 Particle aggregation resulting in clog formation. (a–e) The density matched suspension of polystyrene particles (D = 3 μm) with sulphate charge groups flows through a constriction of width W = 15.5 μm. The images are recorded at 3, 5, 10 and 36 minutes, with a flux of 2.8×10^4 particles per minute at the onset of the experiment. Reprinted with permission from *Microfluid. Nanofluid.*[96] Copyright 2015 Springer. (f–h) Schematic representation of the aggregation process, from the deposition of the first particle to the clog formation.

very sensitive to surface roughness and local defects, which are difficult to describe analytically and numerically.[4]

To model these observations, one has to consider the flux of particles, which satisfies the mass conservation relation:[100]

$$\nabla \cdot j = 0. \tag{9}$$

The particle flux is due to hydrodynamic effects (advection and diffusion) and surface or colloidal interactions. The flux in the i-direction is a function of $\mathscr{D}_i$ and U_i, the particle diffusivity and the velocity in the i-direction, respectively, and F_i is the i-component of the resultant force acting on the particle. For a particle number concentration n, the flux in the i-direction j_i is defined as[100]

$$j_i = -\mathscr{D}_i \frac{\partial n}{\partial i} + U_i n + \frac{\mathscr{D}_i F_i n}{k_B T}, \tag{10}$$

where k_B is the Boltzmann constant and T the absolute temperature.

The resultant force $\boldsymbol{F}$ exerted on a colloidal particle is a combination of the van der Waals, electrical double layer, gravitational and hydrodynamic forces:[101]

$$\boldsymbol{F} = \boldsymbol{F}_{vdW} + \boldsymbol{F}_{EDL} + \boldsymbol{F}_G + \boldsymbol{F}_H. \tag{11}$$

If the radius of curvature of the channel wall is large compared to the radius of the particle, the surface can be considered flat and the forces are normal to the surface, *i.e.*, along the unit normal vector n. Assuming that the suspension is diluted, we consider the particle–particle interactions negligible. The sign and magnitude of these forces depend on the distance between the particle and the surface noted h, and on the surface properties. The forces are described theoretically as:

$$F_{vdW} = -\frac{A_0 \lambda D(\lambda + 22.2h)}{3h^2(\lambda + 11.1h)^2}, \tag{12}$$

$$F_{EDL} = 32\pi\varepsilon\kappa D\gamma_p\gamma_w \exp(-\kappa h)\left(\frac{k_B T}{e}\right)^2, \tag{13}$$

$$F_G = -\frac{1}{6}\pi D^3\left(\rho_p - \rho_f\right) g \cdot n, \tag{14}$$

$$F_H = -\frac{C_D}{8}\rho_f \pi D^2 U\, \boldsymbol{U} \cdot n. \tag{15}$$

In these equations, D is the diameter of the particle, λ is the London retardation wavelength, κ the Debye parameter, and e the fundamental electronic charge. The particle–wall interactions depend on ε the permittivity of the fluid, A_0 is the Hamaker constant for the particle–wall interaction, ρ_p and ρ_f the density of the particle and fluid, respectively. The terms $\gamma_{p/w}$ defined for both the particle and the wall are equal to $\gamma_{p/w} = \tanh[(ze\zeta_{p/w})/(4k_B T)]$ where $\zeta_{p/w}$ is the surface zeta potential and z the valency of the symmetric electrolyte. The relative velocity of the particle in the fluid is noted U and the Stokes drag coefficient C_D.

It is important to note that the diffusion and drag coefficients, $\mathscr{D}$ and C_D respectively, vary with h, when the distance between the particle and the wall becomes small, $h \leq D/2$.[105–108]

At low Reynolds number, when the suspension flows between two parallel plates, the velocity profile is described by Poiseuille law, assuming that the flow is undisturbed by the particles. The flux of particles can then be obtained by solving eqn (11) numerically. The results are in good agreement with the experimental observations.[100] This approach has also been used to determine the deposition rate of particles at the inlet of a channel, where the velocity field is determined numerically.[38,39]

For more complex flow geometries, Wyss *et al.*[30] proposed an empirical description of the deposition probability, which describes the flux of particles at the wall. This probability, noted p_{dep}, at a constriction of width W scales with the number of particles that flow in the vicinity of the wall, in the so-called "sticking region" of thickness ε_s. The probability is defined statistically as

$$p_{dep} \propto \frac{\varepsilon_s}{W}\frac{U_{stick}}{U_{total}}, \tag{16}$$

where U_{stick}/U_{total} is the ratio of the average velocity in the sticking region to the average velocity in the channel, assuming that the flow is laminar. This result is consistent with the approach previously described as the sticking thickness ε_s is an empirical parameter, which effectively captures the particle–wall interactions.

4.2 Successive deposition of particles: growth of an aggregate

The subsequent deposition of particles results from the same competition between hydrodynamic, diffusive and colloidal effects [see Fig. 6(b)–(d), (g) and (h)]. However the presence of previously deposited particles modifies the local geometry of the wall, the flow field and the nature of the interactions. The aggregate buildup is therefore more complex to describe analytically or numerically. Two types of deposition mechanisms have been reported depending on the local interactions.[98] If the interactions between the flowing and the deposited particles are attractive for all separation distances, multiple layers of particles are deposited, which results in the formation of an aggregate and the clogging of the microchannel.[93] If the interactions between flowing and deposited particles are repulsive for a range of separation distances, the electrostatic barrier reduces the probability of deposition. At low flow velocity, the particles can only stick on the wall outside a forbidden region that surrounds each deposited particle. This repulsion prevents the buildup of aggregates. At large enough velocities, the repulsion between particles can be overcome and multi-layered clusters are formed resulting in the growth of aggregate.

In experimental studies, the deposition of the particles and the formation of aggregates is monitored through the total size of the cluster area.[92,93] This measurement records the footprint or projected area of the aggregates on the surface of the channel. For electrostatically neutral particles, the total size of the clusters varies linearly in time and with the particle concentration, until the aggregates start interacting with one another. The growth rate of an aggregate increases with the shear strain rate at the wall and the confinement.[92,93] The shape of the aggregates and their growth dynamics also depend on the Peclet number, which

quantifies the relative magnitude of the advective to the diffusive effects, and the ionic strength of the suspension.[97,109] Using a simplified Smoluchowski equation, it is possible to define theoretically the flux of particles at the wall as

$$j \propto -nn_cK_a, \tag{17}$$

where n is the particle number concentration, n_c the number of clusters at the wall per unit volume and K_a the kernel representing the rate of aggregation of independent particles to existing clusters, which is estimated empirically.[92] The clusters are assumed to be hemispherical, randomly close-packed assemblies of particles, and the volume and the area of the clusters are related: $V_c \propto {A_c}^{3/2}$. Then, for particles of volume V_p in a suspension of solid particles of volume fraction ϕ, we have

$$\frac{dA_c}{dt} \propto \frac{\phi\beta}{V_p\sqrt{A_c}}, \tag{18}$$

where β is the growth coefficient, that is defined empirically, and observed to vary as $\sqrt{A_c}$.[30,92,110] These experimental results and scaling laws do not fully capture the complexity of the aggregate growth including the three dimensional geometry, which results from the complex interplay of aggregation and erosion under microfluidic flows.[97]

4.3 Clogging by aggregate growth

The consequence of the aggregate growth in a microfluidic device or in a confined environment is the formation of a clog. Experimental studies have described the dynamics of clog formation at a constriction through the clogging time. The clogging time aims to establish how the flow characteristics and the properties of the suspension contribute to the blockage of a microchannel. The microfluidic technology enables to reproduce the geometry of porous media in a controlled way. For example, each microchannel can present one[85,94,96] or several constrictions.[30,37,111] The clogging timescale is obtained by recording the fraction of blocked channels during the experiment and defining the mean clogging time as the average clogging time for all the microchannels of the device, measured from the onset of the flow. The average clogging time decreases linearly with the pressure drop across the device and the volume fraction of the suspension.[30,37] Experimental results indicated that the clogging time corresponds to the passage of a critical number of particles through the channel before it clogs. The critical number of particles, N^*, depends on the geometry of the microchannel and scales as W/D where W is the width of the channel and D the particle diameter.[30,96] In first approximation, one can assume that the probability of deposition of the successive particles differs only because of the progressive reduction in microchannel opening. The clog is formed when N^* particles have flown through the constriction, and N particles are deposited on the wall of the channel, forming a clog. Using the statistical method presented above, N^* is defined as

$$N^* = \sum_{n=1}^{n=N} \frac{1}{p_{dep}}, \tag{19}$$

where N is the number of particles needed to geometrically block the microchannel $N \propto WH/D^2$ and

$$p_{dep} \propto \frac{\varepsilon_s U_{stick}}{W_{open} U_{total}} \tag{20}$$

depends on the number of particles obstructing the channel through the open width, W_{open}. Upon summation,

$$N^* \propto \frac{W^3 H}{6D^4}, \tag{21}$$

a result that is in good agreement with experimental results.[30,94,96] The semi-empirical approach presented above allows to predict the rate of clogging of microchannels by successive deposition of particles.

5 Perspectives: bio-clogging

If the microfluidic technology has been key to identify and describe the clogging mechanisms involving colloidal and micrometer-scale particles, it is also a powerful tool to study the flow of biofluids through microchannels. In biological or bioengineered systems, cells in suspensions can be transported through micrometer to centimeter-scale channels.[112–115] The clogging of microchannels by cells is encountered in both healthy and pathological organisms. The complex processes involved have been the focus of recent work.[115,116] Other studies have leveraged the formation of clogs to describe the behavior of cells, and proposed new schemes for diagnostic and treatment testing.[117–119]

For example, the selective blockage or sieving of cancer cells in microchannels has been proposed to diagnose diseases.[9,121,123,124] The bridging of sickle red blood cells in blood vessels has been associated with anemic crisis in millions of patients.[125–127] Finally, the formation of bacterial biofilms and biofilm streamers in porous media is the result of the progressive aggregation of bacteria that can eventually lead to clogging (as illustrated in Fig. 7(a)). Indeed, the formation of biofilms has dramatic consequences including the increased resistance to bactericides which is responsible for persistent infections, and biofouling of flow systems, from catheters to pipelines.[128,129] These three examples of bioclogging have been the focus of recent microfluidic studies that have led to a better understanding of the processes specific to biological systems. The use of microfluidic technology to study and leverage bioclogging is a promising emerging field of work. The richness of bioclogging mechanisms stems from the properties of individual cells that differ from solid particles in the following ways: (i) the cells are soft, most often non-isotropic objects; (ii) the cells adhere to the substrate through specific molecules that decorate the cell membranes and can selectively and strongly bind the cell to the substrate; (iii) the cells are living entities that can swim, multiply, differentiate, recruit other cells and synthesize polymeric substances. To illustrate how these differences modify the clogging dynamics and highlight the role of microfluidic advances in biological research, we describe the examples presented above. Indeed each system shows that the living nature of the cell modifies the clog formation.

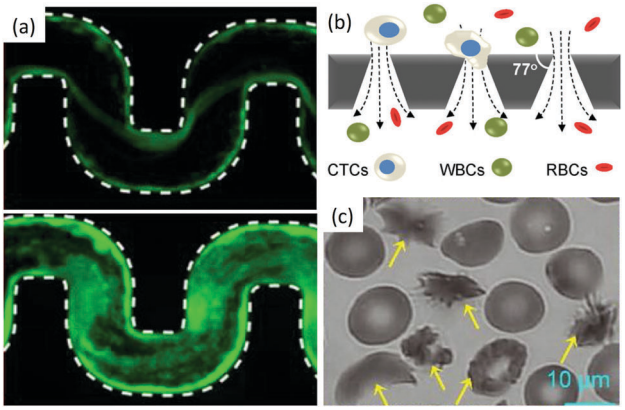

Fig. 7 Bio-clogging. (a) Biofilm streamers of *P. aeruginosa* cells expressing gfp expand and clog a 200 μm wide curvy channel. Reprinted with permission from *Proc. Natl. Acad. Sci. U. S. A.*[120] (b) Schematic of a separation method to isolate Circulating Tumour Cells (CTCs) from other blood cells such as Red Blood Cells (RBCs) and White Blood Cells (WBCs). Reprinted with permission from *Sci. Rep.*[121] Copyright 2014 Nature Publishing Group. (c) Sickled *vs.* healthy red blood cells. The yellow arrows point toward the sickled RBCs. Reprinted with permission from *Proc. Natl. Acad. Sci. U. S. A.*[122]

The sieving of cells in microchannels provides information on their size and mechanical properties (see Fig. 7(b)). Biological research has shown that circulating tumor cells are transported in the peripheral blood of cancer patients and are believed to cause metastasis.[130] Interestingly, the deformability of cancer cells is correlated with their metastatic potential.[131] Therefore, microfluidic devices with conical and narrowing channels have been designed to take advantage of this property and have successfully been used to separate cancer cells from a blood sample using a sieving approach.[9,121,123,124] Once isolated, the cells can be used for diagnostic or therapy tests. This method allows to recover up to 90% of the cancer cells. However, upon clogging, cancer cells attach on the wall of the channel, and the adsorption is irreversible, which limits the use of the device, the ability to analyse the cells trapped.[124] Indeed cells, through the metastatic process adhere to the blood vessel walls. The clogging of the constriction is thus a combination of sieving of soft particles and adhesion to the wall.[130]

The jamming of cells has recently been observed in yeast.[132] In this situation, the formation of force chains results from the growth of the cell population in a confined space and provides environmental cues, but is not associated with fluid flow. The bridging however has been associated with the flow of pathological blood cells.[133] The bridge formation which causes vaso-occlusive crises does not occur when healthy red blood cells (RBCs) flow through a constriction. Yet, for patients affected with sickle cell anemia, a drop in oxygen level in the blood can trigger a series of events that go from the polymerization of hemoglobin S inside the cells to the vessel jamming [see Fig. 7(c)].[125] Studies in microchannels with varying oxygen concentration in the blood flow, reproduce the conditions of the crises in a controlled environment.[117,122,133,134] This work has demonstrated a correlation between the speed of the rheological response of the diseased blood cells and the severity of the crises. However questions remain on the respective role and timescale of the cell stiffness, sickled shape (see Fig. 7(c)) and adhesion properties in the vessel jamming, but the microfluidic technology offers a unique window in this complex dynamical process.

Finally, the aggregation of cells in the wall of microchannels can cause the formation of a clog. For example, the biofouling of porous filtration materials refers to the dramatic flow rate reduction due to the deposition and division of bacteria as well as the synthesis of polymeric substances during the biofilm and biofilm streamers formation.[128,129] Studies in microfluidic devices have revealed information on the biofilm formation and properties and demonstrated that the biofilm streamers are porous structures that filter planktonic cells until clogging.[120,135–137] The new technological platform will allow to study the transition from planktonic to biofilms and the influence of the flow features on the clogging dynamics.

6 Conclusion

In this review, we have reported on recent work that investigated the formation of clogs at the pore-scale level in microfluidic devices. Indeed, over the past decade, the microfluidic technology has been shown to be a powerful tool to control the flow of particles and record the dynamics of clog formation in different channel geometries. This new approach has led to a better description at the pore-scale, *i.e.*, at the scale of a microchannel, of the three clogging mechanisms induced by the flow of micrometer-scale particles: sieving, bridging and aggregation (see Table 1).

Table 1 Clogging in microfluidic systems: mechanisms, suspension properties and channel geometry

	Sieving	Bridging	Aggregation
Size comparison (particle diameter D, channel width W)	$D \geq W$	$D \leq W$	$D \leq W$
Solid volume fraction in suspension ϕ	Low ϕ	Large ϕ	Low ϕ
Interactions needed	Steric	Steric	Attractive particle–wall and particle–particle interactions
Clog formation	Blockage by a single particle	Blockage by an arch of particles	Successive deposition of particles leading to blockage

In summary, sieving and bridging involve steric effects whereas the clogging by aggregation is induced by particle–particle and particle–wall attractive forces. The sieving is observed for particles that have a size D larger or comparable to the width W of the constriction, $W/D \leq 1$, for any concentration of particles. The bridging occurs for suspensions having a large concentration ϕ flowing through narrow microchannel, whose width is typically of the order a few particles radii $W \sim 2$–$10D$. Finally, clogging by aggregation can involve very diluted suspensions and fairly large constrictions but requires particle–wall and particle–particle attraction.

The recent observations performed in microfluidic systems, at the pore-scale, where the coupling between micrometer-scale particles and the microchannel walls can be finely characterized, will allow future investigations. An important step is to build on the microscopic observations performed in one microchannel and study more complex networks of channels, thus bridging the gap between the microfluidic studies and the clogging of porous media and filters that has been extensively studied in the past century at the macroscopic level.

The clogging mechanisms discussed in this review are relevant for colloidal and micrometer-scale particles. These mechanisms are also encountered in biological environments in which cells can block capillaries or microchannels and foul porous media. In particular, the technological applications of clogging to biological and biomedical systems constitute a promising research area, both fundamental as the mechanisms of biofouling are complex, and applied as the formation of biofilms and other cell aggregates have dramatic health consequences.

Acknowledgements

ED acknowledges financial support from the American Chemical Society Petroleum Research Fund under grant agreement PRF # 55845-ND9. The work of AS is partially supported by a CNRS PICS grant no. 07242.

References

1 E. Guazzelli and J. F. Morris, *A Physical Introduction to Suspension Dynamics*, Cambridge University Press, 2011.
2 J. Mewis and N. J. Wagner, *Colloidal Suspension Rheology*, Cambridge University Press, 2012.
3 P. Yang, S. Gai and J. Lin, *Chem. Soc. Rev.*, 2012, **41**, 3679–3698.
4 M. Elimelech, J. Gregory and X. Jia, *Particle Deposition and Aggregation: Measurement, Modelling and Simulation*, Butterworth-Heinemann, 2013.
5 D. A. Fedosov, H. Noguchi and G. Gompper, *Biomech. Model. Mechanobiol.*, 2014, **13**, 239–258.
6 F. Liang, M. Sayed, G. A. Al-Muntasheri, F. F. Chang and L. Li, *Petroleum*, 2016, **2**, 26–39.
7 R. G. M. van der Sman, *Soft Matter*, 2009, **5**, 4376–4387.
8 W. Zhang, X. Tang, N. Weisbrod and Z. Guan, *J. Mt. Sci.*, 2012, **9**, 770–787.
9 L. Pang, S. Shen, C. Ma, T. Ma, R. Zhang, C. Tian, L. Zhao, W. Liu and J. Wang, *Analyst*, 2015, **140**, 7335–7346.
10 J. Gong, R. Jaiswal, P. Dalla, F. Luk and M. Bebawy, *Semin. Cell Dev. Biol.*, 2015, **40**, 35–40.
11 Y. Zhang, H. F. Chan and K. W. Leong, *Adv. Drug Delivery Rev.*, 2013, **65**, 104–120.
12 E. Vignati, R. Piazza and T. P. Lockhart, *Langmuir*, 2003, **19**, 6650–6656.
13 W. Guo, H. H. Ngo and J. Li, *Bioresour. Technol.*, 2012, **122**, 27–34.
14 C. Henry, J. P. Minier and G. Lefevre, *Adv. Colloid Interface Sci.*, 2012, **185–186**, 34–76.
15 W. Zhang, J. Luo, L. Ding and M. Y. Jaffrin, *Ind. Eng. Chem. Res.*, 2015, **54**, 2843–2861.
16 G. D. Martin, S. D. Hoath and I. M. Hutchings, *J. Phys.: Conf. Ser.*, 2008, **105**, 012001.
17 M. Singh, H. M. Haverinen, P. Dhagat and G. E. Jabbour, *Adv. Mater.*, 2010, **22**, 673–685.
18 I. Vermes, E. Steinmetz, L. J. J. M. Zeyen and E. van der Veen, *Diabetologia*, 1987, **30**, 434–436.
19 S.-S. Chang, S. Tu, Y.-H. Lui, V. Savage, S.-P. L. Hwang and M. Roper, 2015, arXiv preprint.
20 D. Katanov, G. Gompper and D. A. Fedosov, *Microvasc. Res.*, 2015, **99**, 57–66.
21 R. Gopal, S. Kaur, Z. Ma, C. Chan, S. Ramakrishna and T. Matsuura, *J. Membr. Sci.*, 2006, **281**, 581–586.
22 D. V. Boger, *Annu. Rev. Chem. Biomol. Eng.*, 2013, **4**, 239–257.
23 M. M. Denn and J. F. Morris, *Annu. Rev. Chem. Biomol. Eng.*, 2014, **5**, 203–228.
24 J. M. Brader, M. E. Cates and M. Fuchs, *Phys. Rev. E: Stat., Nonlinear, Soft Matter Phys.*, 2012, **86**, 1–17.
25 I. E. Zarraga, D. A. Hill and D. T. Leighton, *J. Rheol.*, 2000, **44**, 185–220.
26 C. B. Holmes, M. Fuchs and M. E. Cates, *Europhys. Lett.*, 2003, **63**, 240–246.
27 J. F. Morris, *Rheol. Acta*, 2009, **48**, 909–923.
28 G. During, E. Lerner and M. Wyart, *Phys. Rev. E: Stat., Nonlinear, Soft Matter Phys.*, 2014, **89**, 1–12.
29 G. K. Batchelor, *An Introduction to Fluid Dynamics*, Cambridge university press, 2000.
30 H. Wyss, D. Blair, J. Morris, H. Stone and D. Weitz, *Phys. Rev. E: Stat., Nonlinear, Soft Matter Phys.*, 2006, **74**, 061402.
31 J. C. McDonald and G. M. Whitesides, *Acc. Chem. Res.*, 2002, **35**, 491–499.
32 A. Sauret, E. Barney, A. Perro, E. Villermaux, H. Stone and E. Dressaire, *Appl. Phys. Lett.*, 2014, **105**, 074101.
33 H. M. Wyss, T. Franke, E. Mele and D. a. Weitz, *Soft Matter*, 2010, **6**, 4550–4555.
34 S. L. Sanderson, A. Y. Cheer, J. S. Goodrich, J. D. Graziano and W. T. Callan, *Nature*, 2001, **412**, 439–441.
35 B. V. D. Bruggen, C. Vandecasteele, T. V. Gestel, W. Doyenb and R. Leysenb, *Environ. Prog.*, 2003, **22**, 46–56.
36 B. He, L. Tan and F. Regnier, *Anal. Chem.*, 1999, **71**, 1464–1468.
37 B. Mustin and B. Stoeber, *Microfluid. Nanofluid.*, 2010, **9**, 905–913.

38 J. Lin, D. Bourrier, M. Dilhan and P. Duru, *Phys. Fluids*, 2009, **21**, 1–14.
39 P. Duru and Y. Hallez, *Langmuir*, 2015, **31**, 8310–8317.
40 H. Wei, B.-h. Chueh, H. Wu, E. W. Hall, C.-w. Li, R. Schirhagl, J.-M. Lin and R. N. Zare, *Lab Chip*, 2011, **11**, 238–245.
41 J. Kim, J. Erath, A. Rodriguez and C. Yang, *Lab Chip*, 2014, **14**, 2480–2490.
42 S. J. Blott and K. Pye, *Sedimentology*, 2012, **59**, 2071–2096.
43 C. S. Chern, *Prog. Polym. Sci.*, 2006, **31**, 443–486.
44 B. Liu, M. Zhang, G. Yu, D. Chen and H. Zhang, *Colloids Surf., A*, 2014, **452**, 159–164.
45 R. Pecora, *Dynamic Light Scattering: Applications of Photon Correlation Spectroscopy*, Springer Science & Business Media, 2013.
46 H. Berthet, M. Fermigier and A. Lindner, *Phys. Fluids*, 2013, **25**, 103601.
47 M. Malmsten, *Soft Matter*, 2006, **2**, 760–769.
48 A. Abbaspourrad, N. J. Carroll, S. H. Kim and D. A. Weitz, *J. Am. Chem. Soc.*, 2013, **135**, 7744–7750.
49 M. Destribats, M. Rouvet, C. Gehin-Delval, C. Schmitt and B. P. Binks, *Soft Matter*, 2014, **10**, 6941–6954.
50 M. Abkarian, M. Faivre and H. A. Stone, *Proc. Natl. Acad. Sci. U. S. A.*, 2006, **103**, 538–542.
51 S. She, C. Xu, X. Yin, W. Tong and C. Gao, *Langmuir*, 2012, **28**, 5010–5016.
52 Y. Li, E. Kumacheva and A. Ramachandran, *Soft Matter*, 2013, **9**, 10391–10403.
53 Y. Li, O. S. Saryer, A. Ramachandran, S. Panyukov, M. Rubinstein and E. Kumacheva, *Sci. Rep.*, 2015, **5**, 17017.
54 H. Noguchi, G. Gompper, T. C. Lubensky, H. Noguchit and G. Gompper, *Proc. Natl. Acad. Sci. U. S. A.*, 2016, **102**, 14159–14164.
55 A. S. Popel and P. C. Johnson, *Annu. Rev. Fluid Mech.*, 2005, **37**, 43–69.
56 R. M. Bateman, M. D. Sharpe and C. G. Ellis, *Crit. Care*, 2003, **7**, 359–373.
57 H. Lei and G. E. Karniadakis, *Proc. Natl. Acad. Sci. U. S. A.*, 2013, **110**, 11326–11330.
58 M. Guo and H. M. Wyss, *Macromol. Mater. Eng.*, 2011, **296**, 223–229.
59 T. Kong, L. Wang, H. M. Wyss and H. C. Shum, *Soft Matter*, 2014, **10**, 3271–3276.
60 Q. Guo, S. M. McFaul and H. Ma, *Phys. Rev. E: Stat., Nonlinear, Soft Matter Phys.*, 2011, **83**, 1–5.
61 S. M. McFaul, B. K. Lin and H. Ma, *Lab Chip*, 2012, **12**, 2369–2376.
62 P. Preira, V. Grandné, J.-M. Forel, S. Gabriele, M. Camara and O. Theodoly, *Lab Chip*, 2013, **13**, 161–170.
63 D. J. Hoelzle, B. a. Varghese, C. K. Chan and A. C. Rowat, *J. Visualized Exp.*, 2014, e51474.
64 T.-H. Kim, A. C. Rowat and E. K. Sloan, *Clin. Transl. Immunol.*, 2016, **5**, e78.
65 K. V. Sharp and R. J. Adrian, *Microfluid. Nanofluid.*, 2005, **1**, 376–380.
66 M. E. Cates, J. Wittmer, J.-P. Bouchaud and P. Claudin, *Phys. Rev. Lett.*, 1998, **81**, 1841–1844.
67 A. J. Liu and S. R. Nagel, *Nature*, 1998, **396**, 21–22.
68 M. van Hecke, *J. Phys.: Condens. Matter*, 2010, **22**, 033101.
69 P. G. Lafond, M. W. Gilmer, C. A. Koh, E. D. Sloan, D. T. Wu and A. K. Sum, *Phys. Rev. E: Stat., Nonlinear, Soft Matter Phys.*, 2013, **87**, 1–8.
70 I. Zuriguel, D. R. Parisi, R. C. Hidalgo, C. Lozano, A. Janda, P. A. Gago, J. P. Peralta, L. M. Ferrer, L. A. Pugnaloni, E. Clément, D. Maza, I. Pagonabarraga and A. Garcimartín, *Sci. Rep.*, 2014, **4**, 7324.
71 I. Zuriguel, *Pap. Phys.*, 2014, **6**, 13.
72 A. I. Campbell and M. D. Haw, *Soft Matter*, 2010, **6**, 4688–4693.
73 V. Ramachandran and H. S. Fogler, *J. Fluid Mech.*, 1999, **385**, 129–156.
74 A. Fall, N. Huang, F. Bertrand, G. Ovarlez and D. Bonn, *Phys. Rev. Lett.*, 2008, **100**, 1–4.
75 F. Boyer, É. Guazzelli and O. Pouliquen, *Phys. Rev. Lett.*, 2011, **107**, 188301.
76 J. Paredes, M. A. J. Michels and D. Bonn, *Phys. Rev. Lett.*, 2013, **111**, 015701.
77 T. Divoux, V. Lapeyre, V. Ravaine and S. Manneville, *Phys. Rev. E: Stat., Nonlinear, Soft Matter Phys.*, 2015, **92**, 060301.
78 A. Einstein, *Ann. Phys.*, 1905, **322**, 549–560.
79 G. K. Batchelor, *J. Fluid Mech.*, 1982, **119**, 379–408.
80 D. Genovese and J. Sprakel, *Soft Matter*, 2011, **7**, 3889–3896.
81 A. Deboeuf, G. Gauthier, J. Martin, Y. Yurkovetsky and J. F. Morris, *Phys. Rev. Lett.*, 2009, **102**, 108301.
82 R. Ward and S. G. Whitmore, *Br. J. Appl. Phys.*, 1950, **I**, 325–328.
83 M. D. Haw, *Phys. Rev. Lett.*, 2004, **92**, 185506.
84 L. Isa, R. Besseling, A. N. Morozov and W. C. K. Poon, *Phys. Rev. Lett.*, 2009, **102**, 058302.
85 G. C. Agbangla, E. Climent and P. Bacchin, *Sep. Purif. Technol.*, 2012, **101**, 42–48.
86 U. Zimmermann, F. Smallenburg and H. Löwen, *J. Phys.: Condens. Matter*, 2015, **28**, 244019.
87 G. H. Goldsztein and J. C. Santamarina, *Appl. Phys. Lett.*, 2004, **85**, 4535–4537.
88 J. R. Valdes and J. C. Santamarina, *Appl. Phys. Lett.*, 2007, **90**, 244101.
89 Z. B. Sendekie and P. Bacchin, *Langmuir*, 2016, **32**, 1478–1488.
90 G. M. Whitesides and B. Grzybowski, *Science*, 2002, **295**, 2418–2421.
91 S. Giglia and G. Straeffer, *J. Membr. Sci.*, 2012, **417**, 144–153.
92 M. T. Stamm, T. Gudipaty, C. Rush, L. Jiang and Y. Zohar, *Microfluid. Nanofluid.*, 2011, **11**, 395–403.
93 T. Gudipaty, M. T. Stamm, L. S. L. Cheung, L. Jiang and Y. Zohar, *Microfluid. Nanofluid.*, 2011, **10**, 661–669.
94 S. S. Massenburg, E. Amstad and D. A. Weitz, *Microfluid. Nanofluid.*, 2016, **20**, 94.
95 J. Linkhorst, T. Beckmann, D. Go, A. J. C. Kuehne and M. Wessling, *Sci. Rep.*, 2016, **6**, 22376.
96 B. Dersoir, M. R. de Saint Vincent, M. Abkarian and H. Tabuteau, *Microfluid. Nanofluid.*, 2015, **19**, 953–961.

97 M. R. de Saint Vincent, M. Abkarian and H. Tabuteau, *Soft Matter*, 2016, **12**, 1041–1050.
98 V. Ramachandran and H. S. Fogler, *Langmuir*, 1998, **14**, 4435–4444.
99 G. C. Agbangla, PhD thesis, Universite Toulouse 3, 2011.
100 H. N. Unni and C. Yang, *J. Colloid Interface Sci.*, 2005, **291**, 28–36.
101 J. N. Israelachvili, *Intermolecular and Surface Forces*, Academic press, 2011.
102 H. N. Unni and C. Yang, *Can. J. Chem. Eng.*, 2007, **85**, 609–616.
103 Z. Adamczyk, B. Siwek and L. Szyk, *J. Colloid Interface Sci.*, 1995, **174**, 130–141.
104 M. Elimelech and C. R. O'Melia, *Environ. Sci. Technol.*, 1990, **24**, 1528–1536.
105 H. Brenner, *Adv. Chem. Eng.*, 1966, **6**, 287–438.
106 A. J. Goldman, R. G. Cox and H. Brenner, *Chem. Eng. Sci.*, 1967, **22**, 637–651.
107 A. J. Goldman, R. G. Cox and H. Brenner, *Chem. Eng. Sci.*, 1967, **22**, 653–660.
108 J. Masliyah and S. Bhattacharjee, *Electrokinetic and Colloid Transport Phenomena*, John Wiley & Sons, 2006.
109 C. P. Ortiz, R. Riehn and K. E. Daniels, *Soft Matter*, 2013, **9**, 543–549.
110 E. Brunet, G. Degré, F. Okkels and P. Tabeling, *J. Colloid Interface Sci.*, 2005, **282**, 58–68.
111 T. van de Laar, S. ten Klooster, K. Schroën and J. Sprakel, *Sci. Rep.*, 2016, **6**, 28450.
112 M. Thiriet, *Biology and mechanics of blood flows: Part I: Biology*, Springer Science & Business Media, 2008.
113 M. Thiriet, *Biology and mechanics of blood flows: Part II: Mechanics and medical aspects*, Springer Science & Business Media, 2008.
114 T. A. Duncombe, A. M. Tentori and A. E. Herr, *Nat. Rev. Mol. Cell Biol.*, 2015, **16**, 554–567.
115 C. W. Shields IV, C. D. Reyes and G. P. López, *Lab Chip*, 2015, **15**, 1230–1249.
116 P. Patil, T. Kumeria, D. Losic and M. Kurkuri, *RSC Adv.*, 2015, **5**, 89745–89762.
117 E. Loiseau, G. Massiera, S. Mendez, P. A. Martinez and M. Abkarian, *Biophys. J.*, 2015, **108**, 2623–2632.
118 J. Picot, P. A. Ndour, S. D. Lefevre, W. E. Nemer, H. Tawfik, J. Galimand, L. Da Costa, J. Ribeil, M. De Montalembert, V. Brousse and B. Le Pioufle, *Am. J. Hematol.*, 2015, **4**, 339–345.
119 J. Ciciliano, Y. Sakurai, D. Myers, M. Fay, B. Hechler, S. Meeks, R. Li, J. Dixon, L. Lyon, C. Gachet and W. Lam, *Blood*, 2015, **126**, 817–824.
120 K. Drescher, Y. Shen, B. L. Bassler and H. A. Stone, *Proc. Natl. Acad. Sci. U. S. A.*, 2013, **110**, 4345–4350.
121 Y. Tang, J. Shi, S. Li, L. Wang, Y. E. Cayre and Y. Chen, *Sci. Rep.*, 2014, **4**, 6052.
122 E. Du, M. Diez-Silva, G. J. Kato, M. Dao and S. Suresh, *Proc. Natl. Acad. Sci. U. S. A.*, 2015, **112**, 1422–1427.
123 T. Huang, C.-P. Jia, Jun-Yang, W.-J. Sun, W.-T. Wang, H.-L. Zhang, H. Cong, F.-X. Jing, H.-J. Mao, Q.-H. Jin, Z. Zhang, Y.-J. Chen, G. Li, G.-X. Mao and J.-L. Zhao, *Biosens. Bioelectron.*, 2014, **51**, 213–218.
124 E. S. Park, C. Jin, Q. Guo, R. R. Ang, S. P. Duffy, K. Matthews, A. Azad, H. Abdi, T. Todenhöfer, J. Bazov, K. N. Chi, P. C. Black and H. Ma, *Small*, 2016, **12**, 1909–1919.
125 G. R. Serjeant and B. E. Serjeant, *Sickle Cell Disease*, Oxford university press, 1992.
126 D. Manwani and P. S. Frenette, *Hematology/the Education Program of the American Society of Hematology. American Society of Hematology. Education Program*, 2013, **122**, 3892–3898.
127 M. T. Gladwin, *Lancet*, 2016, **387**, 2565–2574.
128 M. E. Olson, H. Ceri, D. W. Morck, A. G. Buret and R. R. Read, *Can. J. Vet. Res.*, 2002, **66**, 86–92.
129 M. A. Ghannoum, M. Parsek, M. Whiteley and P. Mukherjee, *Microbial Biofilms*, ASM Press, 2015.
130 D. Wirtz, K. Konstantopoulos and P. C. Searson, *Nat. Rev. Cancer*, 2011, **11**, 512–522.
131 R. A. Harouaka, M. Nisic and S.-Y. Zheng, *J. Lab. Autom.*, 2013, **18**, 455–468.
132 M. Delarue, J. Hartung, C. Schreck, P. Gniewek, L. Hu, S. Herminghaus and O. Hallatschek, *Nat. Phys.*, 2016, **12**, 762–766.
133 J. M. Higgins, D. T. Eddington, S. N. Bhatia and L. Mahadevan, *Proc. Natl. Acad. Sci. U. S. A.*, 2007, **104**, 20496–20500.
134 D. Wood, A. Soriano, L. Mahadevan, J. Higgins and S. Bhatia, *Sci. Transl. Med.*, 2012, **4**, 123.
135 L. De La Fuente, E. Montanes, Y. Meng, Y. Li, T. J. Burr, H. C. Hoch and M. Wu, *Appl. Environ. Microbiol.*, 2007, **73**, 2690–2696.
136 A. P. Mosier, A. E. Kaloyeros and N. C. Cady, *J. Microbiol. Methods*, 2012, **91**, 198–204.
137 A. Karimi, D. Karig, A. Kumar and A. M. Ardekani, *Lab Chip*, 2015, **15**, 23–42.

